# Heterostructure Formation from Hydrothermal Annealing of Preformed Nanocrystals

| | |
|---|---|
| Journal: | *Journal of Materials Chemistry A* |
| Manuscript ID: | TA-ART-11-2014-005926.R1 |
| Article Type: | Paper |
| Date Submitted by the Author: | 26-Nov-2014 |
| Complete List of Authors: | Mendonça, Vagner; UFSCar, Química;<br>Dalmaschio, Cleocir; Federal University of Sao Carlos, Chemistry<br>Leite, Edson; Federal University of Sao Carlos, Chemistry<br>Niederberger, Markus; ETH Zurich, Department of Materials<br>Ribeiro, Caue; Empresa Brasileira de Pesquisa Agropecuaria, LNNA; University Federal of São Carlos, Chemistry |
| | |

# Heterostructure Formation from Hydrothermal Annealing of Preformed Nanocrystals

*Vagner R. de Mendonça[1,2], Cleocir J. Dalmaschio[1,3], Edson R. Leite[1], Markus Niederberger[2] and Caue Ribeiro[4]**

1- Department of Chemistry - Federal University of São Carlos, Rod. Washington Luiz, km 235, CEP: 13565-905 São Carlos, SP, Brazil.

2- Department of Materials – ETH Zurich, Vladimir-Prelog-Weg 5, CH-8093 Zurich, Switzerland.

3- Department of Natural Sciences - Federal University of Espírito Santo, Rod. BR 101, km 60, CEP: 29932-540, São Mateus, ES, Brazil.

4- Embrapa CNPDIA, Rua XV de Novembro, 1452, CEP: 13560-970,
São Carlos, SP, Brazil.

## ABSTRACT

One of the primary challenges in obtaining heterostructures is control of the morphology and surface features of the components that are suitable for a specific application. In this sense, the use of preformed nanoparticles as building blocks is interesting. However, to create heterojunctions between preformed nanoparticles, a further calcination step is usually needed that can result in changes in nanoparticle morphology and surface chemistry. Therefore, the main goal of this study was to explore collision-induced heteroaggregation and oriented attachment under hydrothermal conditions to obtain heterostructures from preformed nanoparticles without further thermal treatment or addition of capping agents. We use anatase $TiO_2$ and rutile $SnO_2$ nanoparticles as a model system. A kinetic model based on a diffusion-controlled reaction is adapted to describe the process. For tracking charge migration across the interface and, consequently, heterojunction formation, we employ an indirect method based on the detection of hydroxyl radicals formed over a semiconductor during UV radiation. The rate of hydroxyl radical formation is directly proportional to the photogenerated charge lifetime, which, in turn, depends on the number of heterojunctions formed. The insights presented here suggest the possibility of obtaining the benefits of heterostructures by using nanoparticles with controlled morphology and surface characteristics.

KEYWORDS: heterostructures; photocatalysis; oriented attachment; preformed nanoparticles.

## INTRODUCTION

Among the many applications of oxide semiconductors, photocatalytic activity for many materials has been widely reported.[1,2] This application is strictly related to the excitation of electrons to the conduction band during irradiation, leaving a positive hole in the valence band. These charges are primarily responsible for several oxidation/reduction reactions that take place on the semiconductor surface and are the basis of the photocatalytic process. However, the problem of poor quantum yield caused by the fast recombination of photogenerated charges limits the practicality of this application.[3] Several strategies have been developed to circumvent this problem, among which the association of semiconductors with metals or metal oxides to form heterostructures is particularly promising.[4,5,6,7]

A special feature of heterostructures is the possibility of getting longer lifetimes for photogenerated electron-hole pairs by suppressing recombination and thus allowing the charges to migrate to the semiconductor surface, increasing, therefore, the occurrence of redox reactions over heterostructure surface.[8] Recently, some reviews have summarized the knowledge in this field.[9,10] Nevertheless, the capability of charge separation in a heterostructure can only emerge if the particles are in intimate contact, that is, if there are heterojunctions between them. Heterojunctions are frequently achieved by thermal treatment at high temperatures,[11] which negatively affects the properties of the nanocrystals for specific applications, such as photocatalysis, due to surface dehydroxylation and surface area reduction.

In this context, soft-chemical (such as sol-gel based) methods lead to the production of such heterostructures by single-step methods. However, one of the drawbacks to obtain heterostructures with controlled morphology by such methods is the difficulty of controlling the simultaneous crystallization process of two different components or to modify the surface of one crystalline material with another one, *e.g.* semiconductor or metal.[12] Therefore, the use of preformed nanoparticles with defined composition and properties to build up heterostructures is of interest.

Several reviews summarized the growth of anisotropic homostructures from preformed nanoparticles through the oriented attachment mechanism.[13,14,15,16,] Under hydrothermal annealing, this mechanism is related to the increased number of particle collisions, which confers a statistical nature that is associated with local crystalline alignment.[17,18] This statistical nature[18] and the common occurrence of imperfect alignment[19] suggest that the oriented attachment promoted by hydrothermal annealing may be useful for tailoring heterostructures.[20]

Therefore, the main goal of this study is to analyze heterostructure formation from preformed nanoparticles induced by a heteroaggregation process followed by the oriented attachment of nanoparticles without further thermal treatment or addition of capping agents. The heteroaggregation process is driven by collisions between different nanoparticles during hydrothermal annealing. To test this hypothesis, we chose anatase $TiO_2$ and rutile $SnO_2$ nanoparticles as a model system. Both oxides belong to the same crystal symmetry (tetragonal) and present two molecular units per unit cell (Z=2).[3] Moreover, the oxides have similar lattice parameters in certain crystallographic directions, and the trends of both to form homostructures by aggregation followed by oriented attachment have been extensively studied.[21,22] Therefore, association between the materials may be easier, facilitating formation of heterostructures.[12,23]

## RESULTS AND DISCUSSION

We first synthesized the $TiO_2$ and $SnO_2$ nanoparticles to be used as heterostructures precursors. The characterization of pristine nanoparticles is presented in

Figure 1. The XRD pattern of $TiO_2$, shown in Figure 1(a), corresponds to the anatase phase (PDF#21-1272). The $TiO_2$ nanoparticles show a specific surface area of $87.5 m^2 g^{-1}$. Assuming spherical particles, this specific surface area corresponds to an average diameter of 18.0 nm, in accordance with the size distribution analysis obtained using TEM images, Figures 1(b) and (c), from which an average diameter of 21.6 nm was calculated. For $SnO_2$ nanoparticles, the XRD pattern presented in Figure 1(d) corresponds to the rutile crystalline phase (PDF#41-1445). The specific surface area of $SnO_2$ nanoparticles is $160 m^2 g^{-1}$, equivalent to a diameter of approximately 5.4 nm, assuming spherical nanoparticles. Additionally, this value is in accordance with that obtained from TEM images, 5.12 nm, as presented in Figures 1(e) and (f). The similarity of diameter values obtained by different techniques, presented in Table 1, indicates that the samples are composed of dispersed and not coalesced nanocrystals.

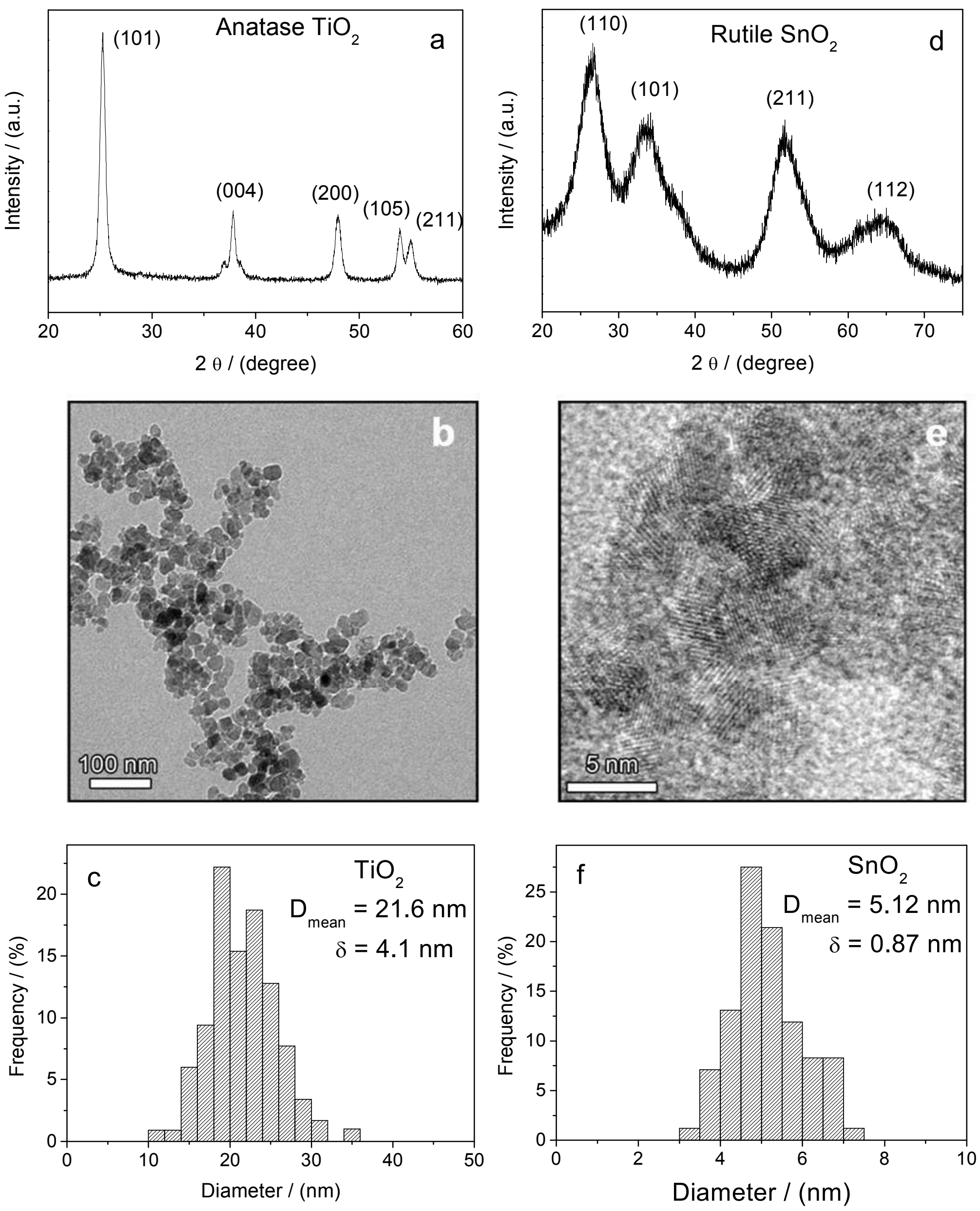

**Figure 1.** Pristine nanoparticle characterization. a) and d) XRD patterns of $TiO_2$ and $SnO_2$ nanoparticles; TEM images of b) $TiO_2$ and e) $SnO_2$ nanoparticles; c) and f) nanocrystal size distribution obtained from TEM images counting at least 150 particles.

**Table 1.** Nanocrystal average diameter obtained by different techniques (size in nm). $^{(1)}$Value not measured

| Sample | XRD | BET | TEM |
|---|---|---|---|
| $TiO_2$ | 15.3 | 18.0 | 21.6 |
| $SnO_2$ | (1) | 5.5 | 5.1 |

An important characteristic of the aqueous suspension containing both preformed anatase $TiO_2$ and rutile $SnO_2$ nanoparticles is that growth by ion/monomer deposition is not supposed to occur; the entire precursor reacts during nanoparticle formation. Moreover, both oxides present very low solubility, preventing/suppressing *Ostwald Ripening* even during hydrothermal annealing.

In this sense, the most likely growth process during the hydrothermal treatment of suspensions containing both oxides is related to collision-induced heteroaggregation and growth by oriented attachment.[20] The process should be spontaneous because the total energy is decreased as a result of the elimination of the solid-liquid interface and an increase in entropy due to desorption of particle surface ligands such as water, protons or hydroxyl groups.[13]

The mechanism for collision-induced aggregation and growth of homostructures under hydrothermal conditions, considering the primary nanoparticles in suspension as molecules, has been described in the literature in the last decade. Penn[13] described the kinetics of oriented aggregation proposing the existence of a rapid equilibrium for the association/dissociation of nanocrystals and an irreversible conversion of associated nanocrystals for producing oriented aggregates. Ribeiro *et al.*[18] developed a kinetic model by considering a diffusion-limited process to describe the oriented attachment of preformed $SnO_2$ nanoparticles. Expanding the ideas presented by Penn and Ribeiro *et* *al.*, both related to the formation of dimers (two aggregated nanoparticles), we derive expressions for the growth of heterostructures in a hydrothermally treated colloidal suspension.

First, we can consider the equilibrium of association/dissociation before heterostructure formation as:

$$A + B \xrightarrow{k_1} AB \qquad \text{Eq. 1}$$

$$AB \xrightarrow{k_1^{'}} A + B \qquad \text{Eq. 2}$$

$$AB \xrightarrow{k_2} P \ , \qquad \text{Eq. 3}$$

where we define A and B as anatase $TiO_2$ and rutile $SnO_2$ nanoparticles, while P represents coalesced nanoparticles containing one point of heterojunction.

Therefore, assuming that the concentration of AB is in a steady state, a second-order rate law can be written:

$$\frac{d[P]}{dt} = \frac{k_1 k_2}{k_1^{'} + k_2}[A][B] \, . \qquad \text{Eq. 4}$$

According to a previous study, after formation of complex AB, coalescence induced by particle rotation may be faster than dissociation,[18] especially due to the cage effect, that is, the lingering of one particle near another on account of the hindering presence of solvent molecules.[24] In this sense, the approximation $k_2 >> k_1^{'}$ can be made, and the reaction becomes a diffusion-limited process.[25] In this process, the global reaction is governed by $k_1$, which can be written as:[26]

$$k_1 = 4\pi N_{AV}(D_A + D_B)R^* \, , \qquad \text{Eq. 5}$$

where $N_{AV}$ is Avogadro’s constant, $D_i$ is the diffusion coefficient of substance $i$ and $R^*$

is the reaction diameter, assumed here as the sum of the particle radius. From the Stokes-Einstein equation an expression for $D_i$ is derived:[27]

$$D_i = \frac{k_B T}{6\pi\eta R_i}. \qquad \text{Eq. 6}$$

Therefore, the equation for $k_1$ can be written as:

$$k_1 = \frac{2}{3}\frac{N_A k_B T}{\eta}\left(2 + \frac{R_A}{R_B} + \frac{R_B}{R_A}\right). \qquad \text{Eq. 7}$$

According to Eq. 7, a higher reaction rate for heterostructure formation occurs between a small particle, which presents high mobility, and a larger particle, which presents a large collision cross section.[28] In this condition, we can consider that the larger particles are stationary with a low collision rate between them, and the smallest particles present a low probability of collision with each other due to their lower reaction cross section. Notably, particles of the same oxide can react with each other, leading to homostructure formation (A + A → AA or B + B → BB). Further reactions, such as P + A → PA, P + B → PB or P + P → PP, are also possible.[29,30]

Pristine nanoparticle characterization shows that $TiO_2$ nanoparticles are approximately 4 times larger in diameter than $SnO_2$ nanoparticles, which corresponds to a rate constant for heteroaggregation, obtained via Eq. 7, that is approximately 3 times higher than the rate constant for homostructure growth, supporting the possibility of heterostructure formation via heteroaggregation of preformed nanoparticles.

As the values for [A] and [B] in Eq. 4 cannot be directly determined, heterostructure assembly was studied using different proportions between oxides during hydrothermal treatment. The $SnO_2$ to $TiO_2$ concentration ratios have to be chosen according to their respective surface areas and their cross sections, because more than one $SnO_2$ nanoparticle can attach to a single $TiO_2$ nanoparticle due to the differences in diameter. With the view to check the oxides proportion in which the reaction of heterostructure formation in maximized, and considering the undefined nature of nanoparticles concentration in such system, the proportions of 10, 20, 35 and 50 wt. % $SnO_2$ were studied.

In order to check the distribution of the two oxides in the samples after hydrothermal treatment at different conditions, we performed EDX analyses at some specific points, highlighted by the red target in Figure 2. For the sample containing 20 wt. % $SnO_2$, analysis at different points presented a proportion of $SnO_2$ between 5.2 and 6.2 wt. %, as shown in Figure 2(a). The deviation from the nominal concentration of 20 wt. % $SnO_2$ points to $SnO_2$ agglomeration, as confirmed in Figure 2(b), where approximately 9-12 wt. % $SnO_2$ is observed in a $TiO_2$ agglomerate, while approximately 55 wt. % $SnO_2$ is observed in a $SnO_2$ agglomerate. Obviously, one part of $SnO_2$ disperses well and gets homogeneously distributed (Fig. 2(a)), whereas one part of $SnO_2$ forms large $SnO_2$ agglomerates, or even does not disperse (Fig. 2(b)). The samples initially containing 50 wt. % $SnO_2$ frequently contained a high number of $SnO_2$ agglomerates with only this oxide after hydrothermal treatment (Figure 2(c)). Additionally, for this sample, $TiO_2$ agglomerates showed a proportion of approximately 10-14 wt. % $SnO_2$. The occurrence of such weak agglomerates is related to the lack of full dispersion of the nanoparticles in suspension before hydrothermal treatment due to the difference in isoelectric points.[31,32] In other words, the weak agglomerates already exist in the suspensions and most likely were not created during hydrothermal treatment. A possibility to circumvent this problem would be the control of nanoparticles surface charges by pH adjustment, aiming a charge-induced heteroaggregation.[7,11] However, in this study, the use of those agents during the hydrothermal treatment was avoided because surface poisoning effects could interfere with further surface measurements.[11]

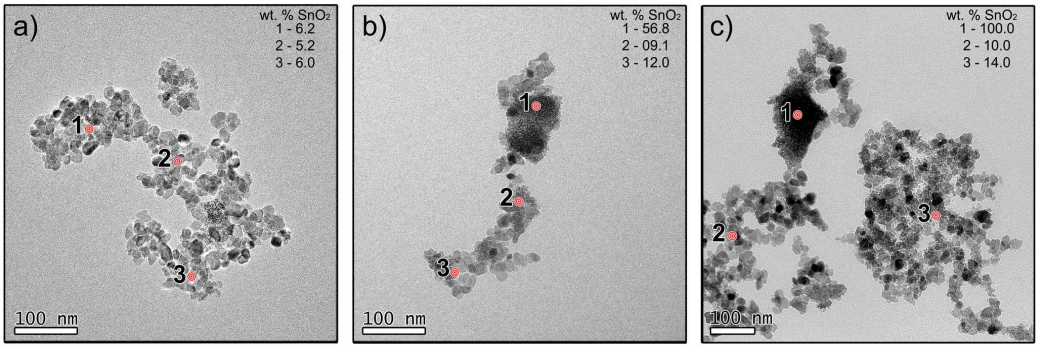

**Figure 2.** TEM images and EDX analyses of selected samples: a) and b) 20 wt. % $SnO_2$; c) 50 wt. % $SnO_2$. The inset of each panel shows the actual wt. % $SnO_2$.

The heteroaggregation procedure seeks the formation of a well-defined interface between two different nanoparticles induced by collisions. These interfaces were analyzed by HRTEM. Figure 3 presents HRTEM images of samples containing 20 wt. % $SnO_2$ hydrothermally treated at 150 °C (Figure 3(a)) and 175 °C (Figure 3(b)). Both samples were treated for 1 h.

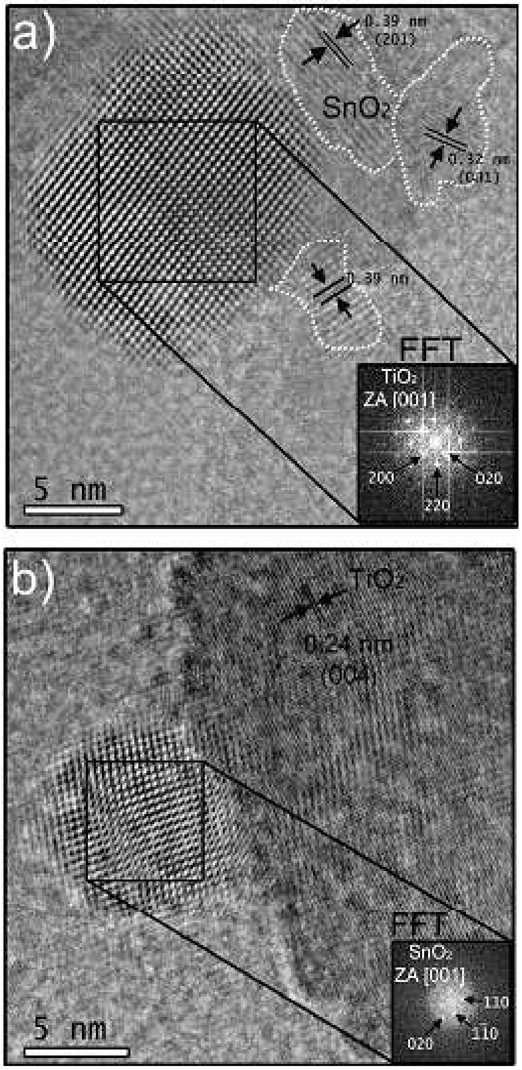

**Figure 3.** High-resolution transmission electron microscopy images for samples containing 20 wt. % $SnO_2$ hydrothermally treated at a) 150 °C and b) 175 °C.

Figure 3(a) depicts $TiO_2$ nanoparticles surrounded by $SnO_2$ nanoparticles. Although the interface is not well defined here, the image shows an important feature of the system: a single $TiO_2$ particle can attach to more than one $SnO_2$ particle. Figure 3(b) shows $TiO_2$ and $SnO_2$ nanoparticles attached to each other with a visible interface between them. The particles can be identified by their different morphologies. The interface is indicative of heterostructure formation. However, from HRTEM analysis, it is not possible to extract statistically relevant information for heterojunctions formation because it requires a large amount of samples, [33] neither infer about the main feature of heterostructures, the charge migration between the oxides. Therefore, indirect techniques are required to verify the formation of heterojunctions that allow charge migration through the interface.

Considering that particles from the same source are used to build up heterostructures, specific features of separated particles, such as surface hydroxylation and crystalline defects, have similar influences on heterostructure properties, independent of hydrothermal treatment conditions, such as oxide proportion, time and temperature. Therefore, one specific property that changes after heterojunction formation is suitable for tracking purposes. For a $TiO_2$-$SnO_2$ heterostructure, photogenerated charges (electron and hole) should migrate to different materials due to their different band-gaps (3.2 eV for $TiO_2$ and 3.8 eV for $SnO_2$), work functions (4.2 and 4.9 eV) and electron affinities (4.0 and 4.5 eV). In the present case, a type-II heterojunction is formed in the staggered arrangement at the oxide interface. Consequently, electrons tend to accumulate in the $SnO_2$ conduction band, while positive holes tend to accumulate in the $TiO_2$ valence band, counteracting charge carrier recombination.[3] A direct consequence of this charge migration is an increase in the lifetime of photogenerated charges, causing an increase in the oxidation reaction rate over the semiconductor surface that is promoted by the positive holes in the valence band.[7,23] Therefore, oxidation reactions promoted by the holes can be useful to confirm heterojunction formation and charge migration between the oxides.

Hydroxyl group adsorbed over the heterostructure surface can be oxidized to hydroxyl radicals by the positive hole that remains in the $TiO_2$ valence band after excitation. The rate of hydroxyl radical formation is directly proportional to the number of holes reaching the photocatalyst surface, which, in turn, depends on the number of heterojunctions formed during heterostructure assembly. The excitation of the oxides, charge transfer process between $TiO_2$ and $SnO_2$ and the formation of hydroxyl radical over the semiconductor are shown in Figure 4(a). Spatial separation is responsible for the increase in photogenerated charge lifetime. Therefore, hydroxyl radical formation during UV irradiation was used to track the number of heterojunctions formed during hydrothermal treatment of the $TiO_2$-$SnO_2$ mixture.

To measure the rate of hydroxyl radical formation, we employed the method described by Ishibashi *et al.*[34] In this method, the fluorescence response of 2-hydroxyterephthalic acid, formed by the reaction between hydroxyl radicals and terephthalic acid, as shown in Figure 4(b), is used to detect the hydroxyl radicals formed. According to previous studies,[35] the reaction yield under the conditions applied in this work is around 35 %. The two main reasons are the fact that the hydroxyl radicals add not only to the ortho-positions of the carboxylate groups, but also to their ipso-positions. Moreover, after the luminescent product formation, continuous oxidation by oxygen might compete with other oxidation reactions. The fluorescence intensity at 425 nm, when the product 2-hydroxyterephthalic acid is excited at 315 nm, is directly proportional to the hydroxyl radical concentration. Accordingly, the same light source was used to excite both the oxides and the fluorescence product.

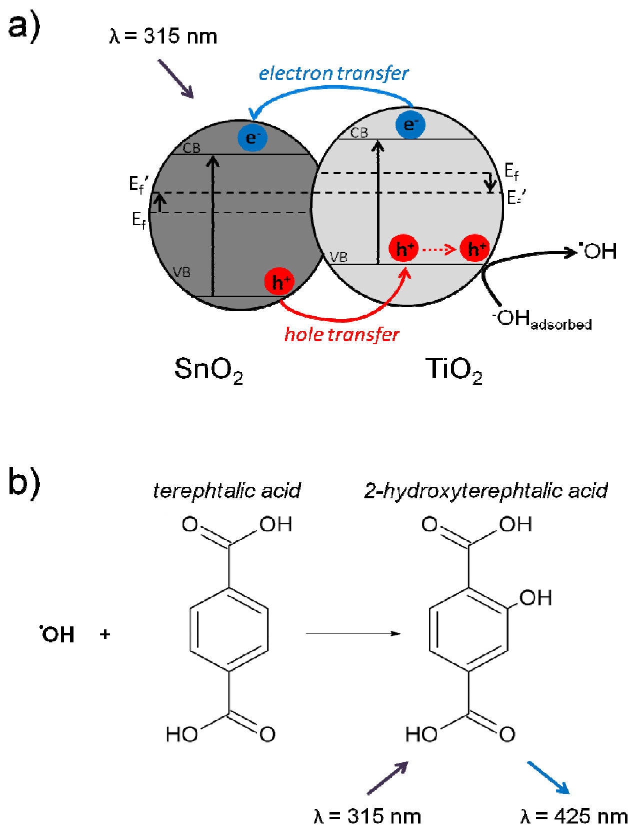

**Figure 4.** a) Band alignment of type-II $TiO_2$-$SnO_2$ heterostructure and formation of hydroxyl radicals. b) The as-formed hydroxyl radical group is detected by the fluorescence response of 2-hydroxyterephthalic acid at λ=425 nm, excited with the same radiation used for oxide excitation (λ=315 nm).

Figure 5(a) shows an example of a set of spectra obtained for one sample. By plotting the maximum of the curve at $\lambda = 425$ nm against time, a straight line is obtained, as shown in Figure 5(b), since the 2-hydroxytherephthalic acid yields should remain the same during the experiments, and the slope ($k_{OH}$) was used to quantitatively evaluate heterojunction formation. Thus, by plotting $k_{OH}$ against different hydrothermal treatment conditions, we can confirm the influence of each condition on heterojunction formation.

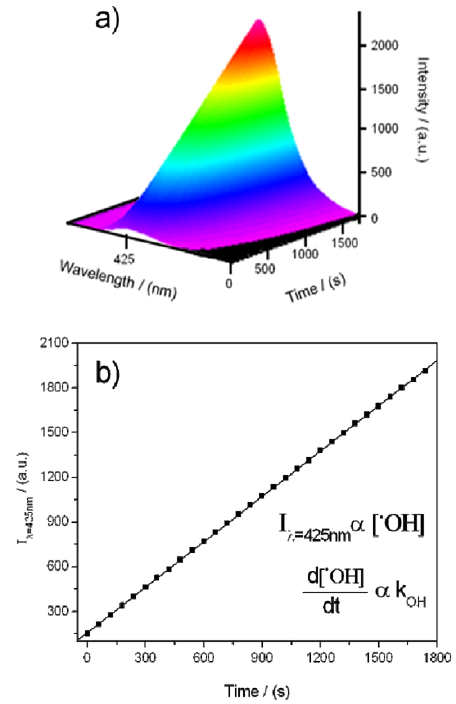

**Figure 5.** PL response of 2-hydroxyterephthalic acid excited at 315 nm. a) Spectra obtained each 60 s with continuous UV irradiation. b) Plot of the maximum intensity against irradiation time. The slope of the curve is directly proportional to $TiO_2$-$SnO_2$ interface formation.

Figure 6 shows $k_{OH}$ plotted against different conditions applied during heterostructure formation by microwave hydrothermal treatment. The $k_{OH}$ curves of treated and pristine $SnO_2$ show inclinations similar to that of the blank experiment, in which only terephthalic acid solution was used; both slopes are near zero. The $SnO_2$ does not exhibit significant photocatalytic activity for hydroxyl radicals generation, most likely due to the relative position (reduction potential) of its conduction band, which is insufficient for reducing molecular oxygen ($O_2 + e^- \rightarrow {}^{\bullet -}O_2$; E° = $-0.33$ eV),[36] facilitating the recombination of photogenerated charges.[37] Since the redox potential values are related to the standard conditions, it is possible the reduction of $O_2$ with electrons from $SnO_2$ conduction band. However, it occurs in a considerably lower rate compared to the other charge transfer processes.[7]

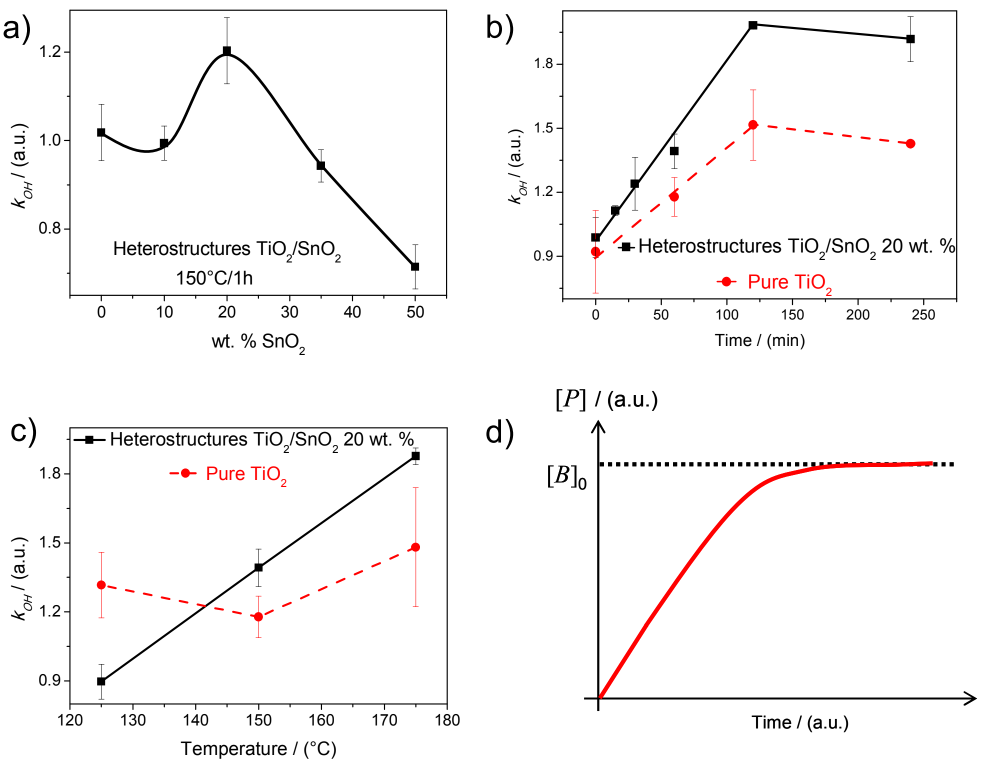

**Figure 6.** Relationship between $k_{OH}$ and specific parameters. a) $k_{OH}$ plotted against $SnO_2$ weight percentage, with all samples treated for 1 h at 150 °C; b) $k_{OH}$ plotted against treatment time for 20 wt. % $SnO_2$ (black line) and pure $TiO_2$ (red line), both treated at 150 °C; c) $k_{OH}$ plotted against treatment temperature for 20 wt. % $SnO_2$ (black line) and pure $TiO_2$ (red line), both treated for 1 h; d) A generic dependence of heterojunction formation with treatment time.

Figure 6(a) presents $k_{OH}$ values according to $SnO_2$ proportion. The $TiO_2$ mass was kept constant in the experiments because it is the active phase for radical formation, and $SnO_2$ in appropriate amounts was added to the suspension. As shown in the plot, there is a maximum at approximately 20 wt. % $SnO_2$. Considering Eq. 4, the 20 wt. % $SnO_2$ sample has the highest $k_{OH}$ value because of the optimized balance between the numbers of nanoparticles of each oxide in terms of concentration, leading to the highest ratio between hetero- and homojunction formation. Since $[P]$ means the number of heterojunctions in Eq. 4, in the reaction at 10 wt. % $SnO_2$, the final value of $[P]$, *i.e.*, the number of heterojunctions formed after thermal annealing, is not sufficient to promote a detectable improvement in the photogenerated charge lifetime by the employed method, which doesn't mean heterojunctions are not formed. The decrease in $k_{OH}$ after the maximum is probably related to the higher $TiO_2$ surface coverage by $SnO_2$, since $SnO_2$ is inactive to hydroxyl radical formation. Another factor that has to be considered is the occurrence of homostructure formation between $SnO_2$ nanoparticles because the number of $SnO_2$ nanoparticles becomes much larger than the number of $TiO_2$ nanoparticles. For instance, when the sample has 35 wt. % of $SnO_2$, due to its lower diameter, the number of $SnO_2$ nanoparticles is around 10 times higher than $TiO_2$ nanoparticles. Therefore, the number of $SnO_2$ particles collision is considerably increased. Moreover, $SnO_2$ homostructure growth is expected because the rate of growth by oriented attachment is strongly size-dependent and increases with the decrease in particle size.[38] It is in accordance with the TEM image and EDX analyses presented in Fig. 2 (c), which show an agglomerate region containing only $SnO_2$. That agglomeration can hamper particle diffusion and collision with $TiO_2$ surfaces, impeding heterostructure formation.

Since 20 wt% $SnO_2$ showed the largest effect on $k_{OH}$, we used this proportion for the following steps. Figure 6(b) shows the relation between $k_{OH}$ and hydrothermal treatment time. For the heterostructures, the value of $k_{OH}$ increases to a limit, after which it remains approximately constant. The decay in $k_{OH}$ with increased hydrothermal treatment time is also possible because junctions between particles of the same species are expected to be formed, based on the kinetic model and previous studies,[18] leading to slightly reduced surface areas. Also, such interfaces act as recombination centers of photogenerated charges.[32,39]

A question that arises from this experiment is whether the increase in $k_{OH}$ with hydrothermal treatment time is related to the formation of new points of heterojunctions or due to the microwave treatment, which could lead to surface or structure modifications. To answer this question, we performed the same experiments using only $TiO_2$. As presented in Figure 6(b), $k_{OH}$ also increases with treatment time but in a lower magnitude than in the samples containing $SnO_2$. The concentration of hydroxyl groups on the $TiO_2$ surface may be affected by microwave heating, leading to an increase in $k_{OH}$ with treatment time. The further possible decrease can also be related to the formation of an interface between $TiO_2$ nanoparticles.[17,32] Therefore we propose that the higher increase in $k_{OH}$ for the heterostructures is related to heterojunction formation and charge migration through the interface between the oxides.

Figure 6(c) shows $k_{OH}$ against hydrothermal treatment temperature for heterostructures containing 20 wt. % $SnO_2$ and pure $TiO_2$, both treated for 1 h. Treatment at 125 °C has a positive effect on pure $TiO_2$ because $k_{OH}$ is higher than that of pristine $TiO_2$, which may be related to the increase of hydroxyl group concentration on the $TiO_2$ surface during the treatment. The $k_{OH}$ value for pure $TiO_2$ is hardly affected by increased treatment temperature. An explanation for the high error range exhibited by pure $TiO_2$ samples may be related to the growth of disordered $TiO_2$ homostructures under thermal treatment, as expected by the developed kinetic model. For the heterostructures, treatment at 125 °C is obviously not sufficient to promote the formation of heterojunctions. There is an energy barrier to the particles attachment and heterojunction formation that is not overcome at this temperature.[17,40] The number of collisions between nanoparticles is another factor that is affected by temperature. Therefore, the lower value of $k_{OH}$ in the heterostructures relative to $TiO_2$ is related to $SnO_2$ coverage without heterojunction formation. There is an increase in $k_{OH}$ with treatment temperature for the heterostructures. This increase can be related to a higher collision rate between the nanoparticles during hydrothermal treatment, which is in accordance with a diffusion-controlled process, as observed in Equation 5. Additionally, the higher rate can result from the energy supplied to overcome the energy barrier that exists in heterojunction formation.

The results presented in Figure 6(b) can be used to analyze the kinetics of the process to infer about the shape of the kinetic curve. Considering the TEM analysis in Figure 3, in which a single $TiO_2$ particle reacts with more than one $SnO_2$ particle, and from Eq. 4, we can consider the concentration of $TiO_2$, [A], constant in the period of time studied. Thus, by limiting a single $SnO_2$ nanoparticle, [B], to creating only one point of heterojunction, [P], it is possible to describe [B] as a function of $[B]_0$, the initial concentration of $SnO_2$, and [P], the concentration of heterojunctions formed during hydrothermal treatment: $[B] = [B]_0 - [P]$. Integrating the rate law using these considerations, we obtain:

$$[P] = [B]_0 (1 - e^{-k't}) , \qquad \text{Eq. 8}$$

where $k' = k_1 \cdot [A]$. Because hydroxyl radical generation is assumed to be proportional to the number of heterojunctions, we can also assume that $[P] \propto k_{OH}$.

A generic plot of this function is shown in Figure 6(d). The function can be correlated to the rate of heterojunction formation, which, in turn, is related to the values of $k_{OH}$ in Figure 6(b). The similarity between this plot and that obtained from the experiments, Figures 6(d) and (b), respectively, is an indicator that the proposed kinetic model for heterojunction formation from preformed nanoparticles under hydrothermal treatment is coherent with the experimental data presented.

## CONCLUSIONS

In summary, we have demonstrated the formation of anatase $TiO_2$ - rutile $SnO_2$ heterostructures from preformed nanoparticles through collisions during microwave hydrothermal treatment. As TEM analyses are not able to unambiguously prove heterojunction formation, we propose an alternative and indirect method based on the detection of hydroxyl radicals formed on crystal surfaces, which is directly related to the number of heterojunctions formed between different nanoparticles. Although the dispersion of small particles of $SnO_2$ over $TiO_2$ is not uniform yet, still leaving room for improvements, we clearly show that their assembly into heterostructures is a versatile way to improve the lifetime of photogenerated electron-hole pairs in semiconductor structures, without the addition of capping agents or calcination steps.

## EXPERIMENTAL SECTION

**Synthesis.** Anatase $TiO_2$ nanoparticles were synthesized by the decomposition of a peroxotitanium complex under hydrothermal conditions, as described in detail in reference 41. Rutile $SnO_2$ nanoparticles were obtained by the hydrolysis of tin (II) chloride dihydrate, as described in detail in reference 31. The synthetic methods were chosen for being surfactant-free, with low counter-ion contamination, and providing materials with defined composition and morphology and narrow size distribution. After the synthesis, the nanoparticles were cleaned with distilled water and freeze-dried to avoid agglomeration.

Heterostructures were prepared by the microwave-assisted hydrothermal treatment of a diluted suspension containing preformed nanocrystals of anatase $TiO_2$ and rutile $SnO_2$ in different proportions, varying treatment time and temperature. The suspensions were prepared from dried nanoparticles precisely mixed in the correct weight ratio. In microwave-assisted treatment, the reaction rate of oriented aggregation dramatically increases in such a system relative to conventional heating.[42,43] The total volume of each reaction was 5 mL, and the concentration of anatase $TiO_2$ was kept constant at 0.8 $g \cdot L^{-1}$, varying only the mass of rutile $SnO_2$ to obtain the required proportion between the oxides. The samples were identified according to the $SnO_2$ mass proportion.

**Characterization.** X-ray diffraction (XRD) analyses were performed with a Rigaku Dmax 2500-PCX X-ray diffractometer with radiation wavelength of 0.15456 nm, corresponding to Cu Kα emission. The $N_2$ physical adsorption at 77 K was studied with a Micromeritics ASAP 2020, and the specific surface areas of the powders were evaluated with the standard BET procedure. For transmission electron microscopy (TEM/HRTEM) and energy-dispersive X-ray (EDX) analyses, a FEI Tecnai G2 F20 microscope operating at 200 kV was used. The samples were prepared by dropping particle suspensions obtained after hydrothermal treatment on a copper grid and left to dry in air.

The $TiO_2$-$SnO_2$ heterostructure is a very active photocatalyst for free radical generation when irradiated with UV light;[3,12] thus, the rate of hydroxyl radical formation was used to indirectly track the number of heterojunctions formed during hydrothermal treatment, since they would be directly proportional. This analysis was performed through the detection of 2-hydroxyterephthalic acid, a highly fluorescent product formed by the reaction between hydroxyl radicals formed over a semiconductor surface under UV radiation and terephthalic acid.[34] For this analysis, suspensions of particles directly from a microwave reactor (5 mL) were added to a solution of terephthalic acid (Aldrich, 98% purity) prepared in 45 mL NaOH (Isofar, 98% purity) so that the final concentrations of terephthalic acid and NaOH were $4\times10^{-4}$ and $2\times10^{-3}$ $mol\cdot L^{-1}$, respectively. Several small portions of the suspensions of each sample after hydrothermal treatment (3 mL) were placed in a fluorimeter with controlled temperature and magnetic stirring (Jasco FP-8500 - Xenon short arc lamp from Ushio - Jasco parts center, Model UXL-159 - with 150 W) and constantly illuminated via the light source of the spectrophotometer with a wavelength of 315 nm. The spectra were collected each 60 s, and the rate of hydroxyl radical formation was assessed by the change of PL intensity at 425 nm emitted from 2-hydroxyterephthalic acid excited by the same spectrophotometer light source at 315 nm. The peak intensity attributed to 2-hydroxyterephthalic acid is proportional to the concentration of hydroxyl radical. The plot of fluorescence intensity against illumination time is linear, and the slope is directly proportional to the rate of hydroxyl radical formation. It was obtained, at least, seven plots of spectrum intensity against irradiation time for each sample. In order to decide which data can be considered to determine $k_{OH}$ average value, we took into account only those with a squared correlation coefficient (R2) higher than 0.999 and we employed the Dixon's Q test, also known as Q test,[44] which is used for identification and rejection of outliers.

## ACKNOWLEDGMENTS

The financial support of FAPESP (Projects 98/14324-0), FINEP, CNPq, CAPES (all Brazilian agencies) and from ETH Zurich is gratefully acknowledged.

## REFERENCES

---

1. Qu, Y. Q.; Duan, X. F. Progress, Challenge and Perspective of Heterogeneous Photocatalysts. *Chem. Soc. Rev.* **2013**, *42*, 2568–2580.

2. Xu, H.; Ouyang, S.; Liu, L.; Reunchan, P.; Umezawa, N.; Ye, J. Recent Advances in TiO2-Based Photocatalysis. J. Mater. Chem. A **2014**, *2*, 12642–12661.

3. Wang, C.; Shao, C.; Zhang, X.; Liu, Y. $SnO_2$ Nanostructures–$TiO_2$ Nanofibers Heterostructures: Controlled Fabrication and High Photocatalytic Properties. *Inorg. Chem.* **2009**, *48*, 7261–7268.

4. Zhou, W. J.; Du, G. J.; Hu, P. G.; Yin, Y. Q.; Li, J. H.; Yu, J. H.; Wang, G. C.; Wang, J. X.; Liu, H.; Wang, J. Y.; Zhang, H. Nanopaper Based on Ag/$TiO_2$ Nanobelts Heterostructure for Continuous–Flow Photocatalytic Treatment of Liquid and Gas Phase Pollutants. *J. Hazard. Mater.* **2011**, *197*, 19–25.

5. Hu, Y.; Li, D. Z.; Zheng, Y.; Chen, W.; He, Y. H.; Shao, Y.; Fu, X. Z.; Xiao, G. C. $BiVO_4$/$TiO_2$ Nanocrystalline Heterostructure: A Wide Spectrum Responsive Photocatalyst Towards the Highly Efficient Decomposition of Gaseous Benzene. *Appl. Catal. B* **2011**, *104*, 30–36.

6. Wang, Y.; Zhang, J. W.; Liu, L. X.; Zhu, C. Q.; Liu, X. Q.; Su, Q. Visible Light Photocatalysis of $V_2O_5$/$TiO_2$ Nanoheterostructures Prepared via Electrospinning. *Mater. Lett.* **2012**, *75*, 95–98.

7. Siedl, N.; Baumann, S. O.; Elser, M. J.; Diwald, O. Particle Networks from Powder Mixtures: Generation of $TiO_2$–$SnO_2$ Heterojunctions via Surface Charge-Induced Heteroaggregation. *J. Phys. Chem. C* **2012**, *116*, 22967–22973.

8. Mahadevu, R.; Yelameli, A. R.; Panigrahy, B.; Pandey, A. Controlling Light Absorption in Charge-Separating Core/Shell Semiconductor Nanocrystals. *ACS Nano* **2013**, *7*, 11055 – 11063.

---

9. Marschall, R. Semiconductor Composites: Strategies for Enhancing Charge Carrier Separation to Improve Photocatalytic Activity. *Adv. Funct. Mater.***2014**, *24*, 2421–2440.

10. Wang, H.; Zhang, L.; Chen, Z.; Hu, J.; Li, S.; Wang, Z.; Liu, J.; Wang, X. Semiconductor Heterojunction Photocatalysts: Design, Construction, and Photocatalytic Performances. *Chem. Soc. Rev.* **2014**, *43*, 5234–5244.

11. Sun, L.; Qi, Y.; Jia, C-J.; Jin, Z.; Fan, W. Enhanced Visible-Light Photocatalytic Activity of g-$C_3N_4/Zn_2GeO_4$ Heterojunctions with Effective Interfaces Based on Band Match. *Nanoscale* **2014**, *6*, 2649–2659.

12. de Mendonça, V. R.; Lopes, O. F.; Fregonesi, R.; Giraldi, T. R.; Ribeiro, C. $TiO_2$-$SnO_2$ Heterostructures Applied to Dye Photodegradation: The Relationship Between Variables of Synthesis and Photocatalytic Performance. *Appl. Surf. Sci.* **2014**, *298*, 181–191.

13. Xue, X.; Penn, R. L.; Leite, E. R.; Huang, F.; Lin, Z. Crystal Growth by Oriented Attachment: Kinetic Models and Control Factors. *CrystEngComm*, **2014**, *16*, 1419–1429.

14. Lv, W. Q.; He, W. D.; Wang, X. N.; Niu, Y. H.; Cao, H. Q.; Dickerson, J. H.; Wang, Z. G. Understanding the Oriented-Attachment Growth of Nanocrystals From an Energy Point of View: A Review. *Nanoscale* **2014**, *6*, 2531–2547.

15. Zhang, J.; Huang, F.; Lin, Z. Progress of Nanocrystalline Growth Kinetics Based on Oriented Attachment. *Nanoscale* **2010**, *2*, 18–34.

16. Niederberger, M.; Helmut, C. Oriented Attachment and Mesocrystals: Non-classical Crystallization Mechanisms Based on Nanoparticle Assembly. *Phys. Chem. Chem. Phys*. **2006**, *8*, 3271–3287.

17. Penn, R. L. Kinetics of Oriented Aggregation. *J. Phys. Chem. B* **2004**, *108*, 12707–12712.

---

18. Ribeiro, C.; Lee, E. J. H.; Longo, E.; Leite, E. R. A Kinetic Model to Describe Nanocrystal Growth by the Oriented Attachment Mechanism. *ChemPhysChem* **2005**, *6*, 690–696.

19. Penn, R. L.; Banfield, J. F. Imperfect Oriented Attachment: Dislocation Generation in Defect-Free Nanocrystals. *Science* **1998**, *281*, 969–971.

20. Ribeiro, C.; Longo, E.; Leite, E. R. Tailoring of Heterostructures in a $SnO_2/TiO_2$ System by the Oriented Attachment Mechanism. *Appl. Phys. Lett.* **2007**, *91*, 103105–1–103105–3.

21. Polleux, J.; Pinna, N.; Antonietti, M.; Niederberger, M. Ligand-Directed Assembly of Preformed Titania Nanocrystals into Highly Anisotropic Nanostructures. *Adv. Mater.* **2004**, *16*, 436–439.

22. Song, H.; Lee, K. H.; Jeong, H.; Um, S. H.; Han, G. S.; Jung, H. S.; Jung, G. Y. A Simple Self-Assembly Route to Single Crystalline $SnO_2$ Nanorod Growth by Oriented Attachment for Dye Sensitized Solar Cells. *Nanoscale*, **2013**, *5*, 1188–1194.

23. Li, Y.; Zhu, L.; Guo, Y.; Song, H.; Lou, Z,. Ye, Z. A New Type of Hybride Nanostructure: Complete Photo-Generated Carrier Separation and Ultrahigh Photocatalytic Activity. *J. Mater. Chem. A* **2014**, *2*, 14245–14250.

24. Atkins, P.; Paula, J. *Physical Chemistry*, 8th ed, W.H. Freeman Company, New York, 2006, p. 876.

25. Xue, X.; Penn, R. L.; Leite, E. R.; Huang, F.; Lin, Z. Crystal Growth by Oriented Attachment: Kinetic Models and Control Factors. *CrystEngComm*, **2014**, *16*, 1419–1429.

26. Calef, D. F.; Deutch, J. M. Diffusion-Controlled Reactions. *Ann. Rev. Phys. Chem.* **1983**, *34*, 493.

---

27. Yang, L. Validity of Nernst-Einstein and Stokes-Einstein Relationships in Molten $NaNO_2$. *J. Chem. Phys*. **1957**, *27*, 601–602.

28. Hawa, T.; Zachariah, M. R. Coalescence Kinetics of Unequal Sized Nanoparticles. *J. Aeros. Sci.* **2006**, *37*, 1–15.

29. Ribeiro, C.; Lee, E. J. H.; Longo, E.; Leite, E. R. Oriented Attachment Mechanism in Anisotropic Nanocrystals: A "Polymerization" Approach. *ChemPhysChem* **2006**, *7*, 664–670.

30. Zhang, J.; Lin, Z.; Lan, Y. Z.; Ren, G. Q.; Chen, D. G.; Huang, F.; Hong, M. C. A Multistep Oriented Attachment Kinetics: Coarsening of ZnS Nanoparticle in Concentrated NaOH. *J. Am. Chem. Soc.* **2006**, *128*, 12981–12987.

31. Ribeiro, C; Lee, E. J. H.; Giraldi, T. R.; Longo, E.; Varela, J. A.; Leite, E. R. Study of Synthesis Variables in the Nanocrystal Growth Behavior of Tin Oxide Processed by Controlled Hydrolysis. *J. Phys. Chem. B* **2004**, *108*, 15612–15617.

32. de Mendonça, V. R.; Ribeiro, C. Influence of TiO2 Morphological Parameters in Dye Photodegradation: A Comparative Study in Peroxo-Based Synthesis. *Appl. Catal. B* **2011**, *105*, 298–305.

33. Burrows, N. D.; Yuwono, V. M.; Penn, R. L. Quantifying the Kinetics of Crystal Growth by Oriented Aggregation. *MRS Bulletin* **2010**, *35*, 133–137.

34. Ishibashi, K.; Fujishima, A.; Watanabe, T.; Hashimoto, K. Detection of Active Oxidative Species in TiO2 Photocatalysis Using the Fluorescence Technique. *Electrochem. Comm.* **2000**, *2*, 207–210.

35. Fang, X.; Mark, G.; von Sonntag, C. OH radical formation by ultrasound in aqueous solutions Part I: the chemistry underlying the terephthalate dosimeter. *Ultrason. Sonochem.* **1996**, *3*, 57–63.

36. M. Grätzel, Photoelectrochemical Cells. *Nature* **2001**, *414*, 338–344.

---

37. Lee, K-T.; Lin, C-H.; Lu, S-Y. $SnO_2$ Quantum Dots Synthesized with a Carrier Solvent Assisted Interfacial Reaction for Band-Structure Engineering of $TiO_2$ Photocatalysts. *J. Phys. Chem. C*, **2014**, *118*, 14457–14463.

38. Penn, R. L.; Tanaka, K.; Erbs, J. Size Dependent Kinetics of Oriented Aggregation. *J. Cryst. Grow.* **2007**, *309*, 97–102.

39. Siedl, N.; Elser, M. J.; Bernardi, J.; Diwald, O. Functional Interfaces in Pure and Blended Oxide Nanoparticle Networks: Recombination versus Separation of Photogenerated Charges. *J. Phys. Chem. C* **2009**, *113*, 15792–15795.

40. Huang, F.; Zhang, H. Z.; Banfield, J. F. Two-Stage Crystal-Growth Kinetics Observed during Hydrothermal Coarsening of Nanocrystalline ZnS. *Nano Lett.* **2003**, *3*, 373–378.

41. Ribeiro, C.; Barrado, C. M.; Camargo, E. R.; Longo, E.; Leite, E. R. Phase Transformation in Titania Nanocrystals by the Oriented Attachment Mechanism: The Role of the pH Value. *Chem. Eur. J.* **2009**, *15*, 2217–2222.

42. Dalmaschio, C. J.; Ribeiro, C.; Leite, E. R. Impact of the Colloidal State on the Oriented Attachment Growth Mechanism. *Nanoscale* **2010**, *2*, 2336–2345.

43. Godinho, M.; Ribeiro, C.; Longo, E.; Leite, E. R. Influence of Microwave Heating on the Growth of Gadolinium-Doped Cerium Oxide Nanorods. *Cryst. Growth Des.* **2008**, *8*, 384–386.

44. Rorabacher, D. B. Statistical Treatment for Rejection of Deviant Values: Critical Values of Dixon's "Q" Parameter and Related Subrange Ratios at the 95 % Confidence Level. *Anal. Chem.*, **1991**, *63*, 139–146

# Heterostructure formation from hydrothermal annealing of preformed nanocrystals

Vagner R. de Mendonça, Cleocir J. Dalmaschio, Edson R. Leite, Markus Niederberger

and Caue Ribeiro

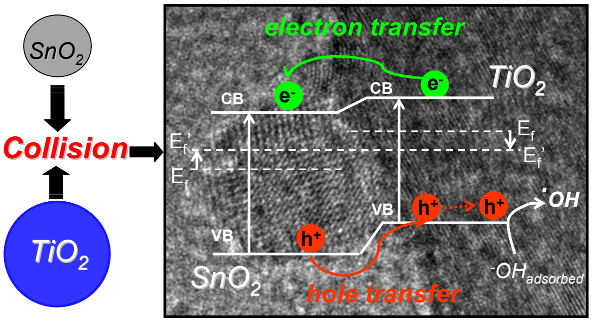

The collision-induced heteroaggregation is a versatile way to obtain the benefits of heterostructures by using nanoparticles with controlled morphology and surface characteristics.